A Computationally Efficient Robust Direct Model Predictive Control for Medium Voltage Induction Motor Drives

Andrei Tregubov, *Student Member, IEEE*, Petros Karamanakos, *Senior Member, IEEE*, and Ludovico Ortombina, *Member, IEEE*

***Abstract*—Long-horizon direct model predictive control (MPC) has pronounced computational complexity and is susceptible to parameter mismatches. To address these issues, this paper proposes a solution that enhances the robustness of long-horizon direct MPC, while keeping its computational complexity at bay. The former is achieved by means of a suitable prediction model of the drive system that enables the effective estimation of the total leakage inductance of the machine. For the latter, the objective function of the MPC problem is formulated such that, even though the drive behavior is computed over a long prediction interval, only a few changes in the candidate switch positions are considered. The effectiveness of the proposed approach is demonstrated with a medium-voltage (MV) drive consisting of a three-level neutral point clamped (NPC) inverter and an induction machine (IM).**

I. Introduction

Over the last years, the advanced processing capabilities of modern microprocessors, combined with a growing demand for high-efficiency variable speed drive (VSD) systems have stimulated the increasing interest of the power electronics community in model predictive control (MPC). This is reflected, e.g., in the exponential growth of publications on the topic since the early 2000s. The most extensively covered MPC method by academia is direct MPC with reference tracking, also known as finite control set MPC (FCS-MPC) [1].

Despite the fact that FCS-MPC appears as an attractive alternative to established control methods [2], it has intrinsic drawbacks. One of them stems from the fact that the computational complexity of the optimization problem underlying FCS-MPC increases exponentially with the length of the prediction horizon. As a result, one-step horizon is typically used, but, alas, at the expense of improved performance and guaranteed stability that long horizons can offer [1], [3]. Even though, there have been some methods that attempt to facilitate the real-time implementation of long-horizon FCS-MPC, such as dedicated branch-and-bound techniques [4], or prediction horizons of nontrivial form [5], keeping the associated computational load (relatively) low remains a challenge [6].

Another drawback of FCS-MPC is that its performance is dependent on the accuracy of the prediction model. The latter, even though typically accurate when power electronic applications are of interest, is subject to model variations and mismatches, that can adversely affect the system performance, especially when long horizons are employed [6]. Hence, FCS-MPC needs to be equipped with tools that can enhance its robustness to such uncertainties. To this end, MPC can be augmented with an element of integrating nature [7], or an external disturbance observer [8]–[10].

An alternative is to employ system identification algorithms. Such methods are either white-box model-based approaches, since they assume full knowledge of the system [11]–[13], or they do not depend on the model at all, i.e., they are black-box methods [14], [15]. The former techniques, however, cannot simultaneously estimate all the system parameters, meaning that combinations of different sources of uncertainties/model mismatches are usually not considered. As a result, the performance of such methods is not the most desired for a wide range of operating conditions. As for the black-box methods, they require measurements of the input (e.g., applied voltage) and output (e.g., load current) and intrinsic look-up tables. Moreover, the acquired data are processed by computational demanding identification techniques, such as data fitting methods, which further increase the computational requirements of MPC. Hence, as can be understood, it is desired that the aforementioned auxiliary tools should come with low computational complexity not to further tax the already high computational load of long-horizon FCS-MPC.

Motivated by the above, this paper proposes a long-horizon FCS-MPC for medium-voltage (MV) induction motor (IM) drives that (a) has modest computational complexity, and (b) shows a high degree of robustness. To achieve the former, the MPC problem is formulated by taking advantage of the fact that MV drives need to operate at low switching frequencies of a few hundred hertz. The latter is accomplished by deriving a prediction model of the drive system that allows for the adoption of a simple, yet effective, estimation algorithm. The presented results, based on an MV drive that consists of a three-level neutral point clamped (NPC) inverter and an IM, highlight the potential of the proposed approach.

II. Modeling

To derive the model of the MV VSD (Fig. 1) that will serve as a prediction model for the FCS-MPC algorithm,

A. Tregubov and P. Karamanakos are with the Faculty of Information Technology and Communication Sciences, Tampere University, 33101 Tampere, Finland; e-mail: andrei.tregubov@tuni.fi, p.karamanakos@ieee.org

L. Ortombina is with the Department of Industrial Engineering, University of Padova, 35122 Padova, Italy; e-mail: ludovico.ortombina@unipd.it

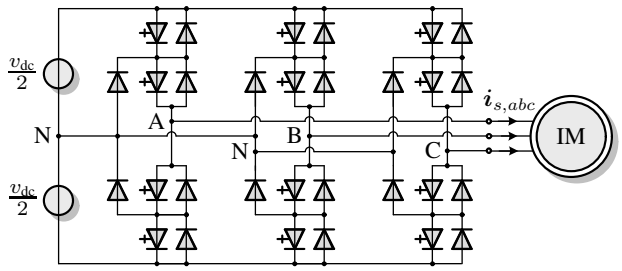

Fig. 1: Three-level NPC converter driving an IM.

the differential equations that fully describe its dynamics are required. To do so, the per unit (p.u.) system and the $\alpha\beta$-reference frame are adopted in this work. Moreover, for simplicity, the neutral point potential v_n is assumed to be zero and the dc-link voltage constant and equal to V_{dc}.

Based on the above, the inverter output voltage $\boldsymbol{v}_{\text{inv}}$ (which is equal to the stator voltage $\boldsymbol{v}_s$) is[1]

$$\boldsymbol{v}_{\text{inv}} = \boldsymbol{v}_s = \frac{V_{\text{dc}}}{2}\tilde{\boldsymbol{K}}\left[u_a \ u_b \ u_c\right]^T, \tag{1}$$

where $\tilde{\boldsymbol{K}}$ is the reduced Clarke transformation matrix

$$\tilde{\boldsymbol{K}} = \frac{2}{3}\begin{bmatrix} 1 & -\frac{1}{2} & -\frac{1}{2} \\ 0 & \frac{\sqrt{3}}{2} & -\frac{\sqrt{3}}{2} \end{bmatrix}, \tag{2}$$

and $\boldsymbol{u}_{abc} = [u_a \ u_b \ u_c]^T$ is the three-phase switch position, with $u_x \in \mathcal{U} = \{-1, 0, 1\}$, $x \in \{a, b, c\}$, being the single-phase switch position.

Regarding the IM, when FCS-MPC algorithms are of interest, the machine is most commonly modeled based on the T-equivalent model, see Fig. 2(a) [16]. In this model, R_s and R_r stand for the stator and rotor resistances, respectively, while X_{ls}, X_{lr}, and X_m are the stator leakage, rotor leakage, and mutual reactances, respectively. However, this model is overparametrized, while observability and identifiability of the machine parameters are not achieved [17]. These issues, nonetheless, can be tackled when using the so-called inverse-Γ model, shown in Fig. 2(b). Note that the two representations of the IM are equivalent and no loss of information or accuracy is entailed [18].

The derivation of the inverse-Γ model is based on providing the same input impedance as the T-model. Hence, the stator voltage $\boldsymbol{v}_s$, current $\boldsymbol{i}_s$, and flux $\boldsymbol{\psi}_s$ are the same in both IM representations. Moreover, the rotor current and flux are defined with the help of the transformation coefficient $\gamma = X_m/X_r$ as $\bar{\boldsymbol{i}}_r = \boldsymbol{i}_r/\gamma$ and $\bar{\boldsymbol{\psi}}_r = \gamma\boldsymbol{\psi}_r$, where the overline denotes variables in the inverse-Γ model, and $X_r = X_{lr} + X_m$. Based on the above definitions, the equivalent circuit representation in Fig. 2(b) is obtained with the following parameters

[1]Note that to simplify the notation, the subscript for variables in the $\alpha\beta$-plane is omitted. Variables in the abc-plane are indicated by the corresponding subscript.

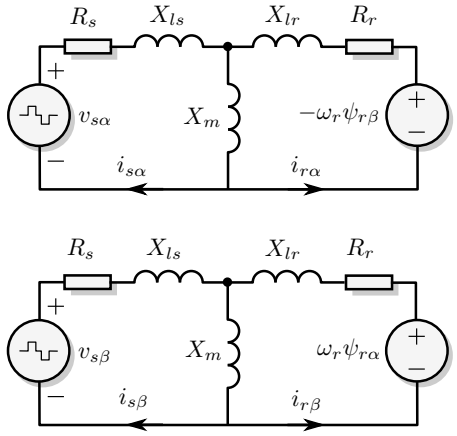

(a) T-model

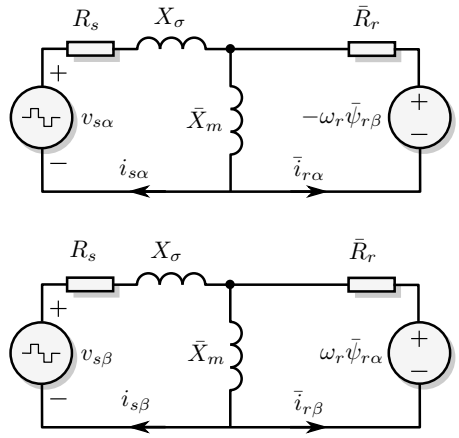

(b) Inverse-Γ model

Fig. 2: Equivalent models of an IM.

$$\bar{X}_m = \gamma X_m\,, \tag{3a}$$
$$\bar{R}_r = \gamma^2 R_r\,, \tag{3b}$$
$$X_\sigma = X_s - X_m^2/X_r\,, \tag{3c}$$

where X_σ is the total leakage reactance, and $X_s = X_{ls} + X_m$.

By comparing Figs. 2(a) and 2(b), one important observation can be made. Namely, the impact of the rotor X_{lr} and stator X_{ls} leakage reactances in the T-equivalent model is mostly captured by the total leakage reactance X_σ in the inverse-Γ model, see (3c). This will be utilized when designing the estimation algorithm, see Section V.

Given the equivalent circuit in Fig. 2(b), the state-space model of the MV drive system can be derived. Specifically, by defining the three-phase switch position $\boldsymbol{u}_{abc} \in \boldsymbol{\mathcal{U}} = \mathcal{U}^3$ as the input of the system, the stator current and flux as state variables, i.e., $\boldsymbol{x} = [\boldsymbol{i}_s^T \ \boldsymbol{\psi}_s^T]^T \in \mathbb{R}^4$, and the stator current as the system output, i.e., $\boldsymbol{y} = \boldsymbol{i}_s \in \mathbb{R}^2$, the continuous-time state-space model can be derived by applying circuit analysis to the inverse-Γ model in Fig. 2(b), i.e.,

$$\frac{\mathrm{d}\boldsymbol{x}(t)}{\mathrm{d}t} = \mathbf{F}\boldsymbol{x}(t) + \mathbf{G}\boldsymbol{u}_{abc}(t) \tag{4a}$$
$$\boldsymbol{y}(t) = \mathbf{C}\boldsymbol{x}(t), \tag{4b}$$

where $\mathbf{F} \in \mathbb{R}^{4\times4}$, $\mathbf{G} \in \mathbb{R}^{4\times3}$ and $\mathbf{C} \in \mathbb{R}^{2\times4}$ are

$$\mathbf{F} = \begin{bmatrix} -\frac{1}{\tau_{s,\Gamma}} & -\omega_\mathrm{r} & \frac{\bar{R}_r}{X_\sigma X_m} & \frac{\omega_\mathrm{r}}{X_\sigma} \\ \omega_\mathrm{r} & -\frac{1}{\tau_{s,\Gamma}} & -\frac{\omega_\mathrm{r}}{X_\sigma} & \frac{\bar{R}_r}{X_\sigma X_m} \\ -R_s & 0 & 0 & 0 \\ 0 & -R_s & 0 & 0 \end{bmatrix}, \text{ with}$$

ω_r being the rotor angular speed, $\tau_{s,\Gamma}$ given by

$$\frac{1}{\tau_{s,\Gamma}} = \frac{\bar{R}_r}{\bar{X}_m} + \frac{\bar{R}_r + R_s}{X_\sigma}, \text{ and}$$

$$\mathbf{G} = \frac{V_\mathrm{dc}}{2X_\sigma}\begin{bmatrix} \boldsymbol{I}_2 & \mathbf{0}_{2\times2} \end{bmatrix}^T \tilde{\boldsymbol{K}}, \qquad \mathbf{C} = \begin{bmatrix} \boldsymbol{I}_2 & \mathbf{0}_{2\times2} \end{bmatrix}.$$

Note that the state $\boldsymbol{x}$ in (4) does not depend on the leakage rotor reactance X_{lr} incorporated in the γ coefficient since, as mentioned, the stator current and flux are the same in both models. This greatly benefits the design of the parameter estimation algorithm in Section V, since knowledge of X_{lr} is not required. Finally, to derive the prediction model for the FCS-MPC algorithm, (4) is discretized with the sampling interval T_s. To this end, exact discretization is used, yielding

$$\boldsymbol{x}(k+1) = \mathbf{A}\boldsymbol{x}(k) + \mathbf{B}\boldsymbol{u}_{abc}(k) \tag{5a}$$

$$\boldsymbol{y}(k) = \mathbf{C}\boldsymbol{x}(k), \tag{5b}$$

where $\mathbf{A} = \mathbf{e}^{\mathbf{F}T_s}$, and $\mathbf{B} = -\mathbf{F}^{-1}(\boldsymbol{I}_4 - \mathbf{A})\mathbf{G}$, with $\mathbf{e}$ being the matrix exponential and $k \in \mathbb{N}$. Finally, it is worth mentioning that in case of an increased computational load, the forward Euler discretization method can be used instead to discretize (4) [6].

III. Controller Design

In this section the formulation of the optimization problem underlying FCS-MPC is presented. Moreover, the effectiveness of the proposed objective function is assessed in terms of the product of the produced stator current distortions and the switching frequency.

A. Optimization Problem

The first aim of the controller is to track the stator current reference $\boldsymbol{i}_{s,\mathrm{ref}}$, i.e., to minimize the tracking error $\boldsymbol{i}_{s,\mathrm{err}} = \boldsymbol{i}_{s,\mathrm{ref}} - \boldsymbol{i}_s$, while the second one is to minimize the switching frequency, i.e., the control effort $\Delta\boldsymbol{u}_{abc}(\ell) = \boldsymbol{u}_{abc}(\ell) - \boldsymbol{u}_{abc}(\ell-1)$. The former objective relates to the current distortions, which have to be kept low for reduced thermal losses, while the latter to the switching power losses, which for an MV drive have to be as low as possible. These objectives are captured in the following objective function

$$J = \sum_{\ell=k}^{k+N_p-1} \|\boldsymbol{i}_{s,\mathrm{err}}(\ell+1)\|_2^2 + \lambda_u \sum_{\ell=k}^{k+N_c-1} \|\Delta\boldsymbol{u}_{abc}(\ell)\|_2^2, \tag{6}$$

where $\lambda_u > 0$ sets the trade-off between the two terms of (6), i.e., the current distortions and the switching frequency. Moreover, N_p denotes the prediction horizon, i.e., the time window wherein the future current trajectories are computed, and N_c is the control horizon, i.e., the time window wherein the possible future control actions are evaluated.

The controller finds the *optimal* sequence of control actions

$$\boldsymbol{U}^*(k) = \begin{bmatrix} \boldsymbol{u}_{abc}^{*T}(k) & \boldsymbol{u}_{abc}^{*T}(k+1) & \dots & \boldsymbol{u}_{abc}^{*T}(k+N_c-1) \end{bmatrix}^T$$

by solving the following optimization problem

$$\underset{\boldsymbol{U}(k)}{\text{minimize}} \quad J(k) \tag{7a}$$

$$\text{subject to} \quad (5) \tag{7b}$$

$$\boldsymbol{U}(k) \in \mathbb{U} \tag{7c}$$

$$\|\Delta\boldsymbol{u}(\ell)\|_\infty \leq 1, \forall \ell = k, \dots, k+N_c-1, \tag{7d}$$

where $\mathbb{U} = \boldsymbol{\mathcal{U}} \times \cdots \times \boldsymbol{\mathcal{U}}$ is the $3N_c$-times Cartesian product of the set $\boldsymbol{\mathcal{U}}$, and represents the feasible input set.

Problem (7) is typically solved by evaluating all possible solutions, i.e., 3^{3N_c}, to conclude to the one that results in the minimum value of (6), i.e., the minimum current error and switching effort. Doing this, however, in real time within a few microseconds can be computationally intractable. To keep the computational complexity low—in contrast to FCS-MPC implementations where $N_p = N_c$, see [1] and references therein—we propose to use two different horizons, i.e., $N_c < N_p$. This approach is tailored to the needs of MV drive systems since, due to the targeted low switching frequencies, only a few changes in the control action are anticipated within the control horizon. Considering that the first steps of the horizon are of more interest since—according to the receding horizon policy [16]—only $\boldsymbol{u}_{abc}^*(k)$ is applied to the inverter, keeping the same control action for the last $N_p - N_c$ steps of the prediction horizon will not adversely affect the system performance. Hence, with the proposed approach a favorable performance of the drive is still achieved (since the prediction horizon N_p remains sufficiently long), while the complexity of the optimization problem underlying long-horizon FCS-MPC remains reasonable (since the control horizon N_c can be kept relatively short), rendering its real-time implementation feasible. Moreover, to further reduce the computational burden of the MPC problem, more sophisticated solving methods, e.g., the sphere decoder [4], [19], can be employed, if needed.

B. Assessment of the Objective Function

To evaluate the performance of the proposed objective function (6), the product of the current total harmonic distortion (THD) I_THD and the switching frequency f_sw is used as a metric, i.e., $c_f = I_\mathrm{THD} \cdot f_\mathrm{sw}$. A lower c_f indicates a favorable steady-state control behavior. The parameters of the drive system are given in Table I, while the sampling interval is $T_s = 25\,\mu$s. Note that the total leakage reactance is $X_\sigma = 0.25$ p.u. The metric is shown in Fig. 3 for FCS-MPC with four different horizon combinations $N = \{N_p, N_c\}$ and nominal parameters in the prediction model.

Based on Fig. 3, some noteworthy observations can be made. First, for frequencies below 500 Hz—which is the most relevant range for MV applications—a long horizon, such as the combination $N = \{5, 2\}$ or $N = \{5, 5\}$,

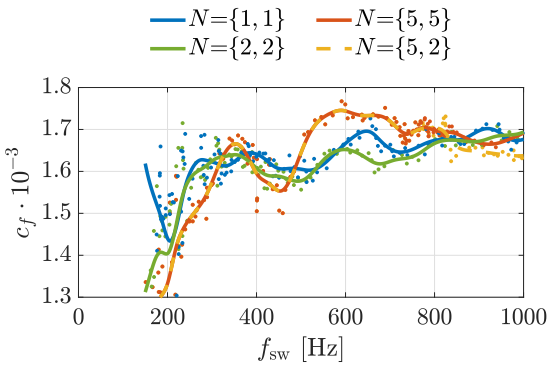

(a) Full range of studied f_{sw}

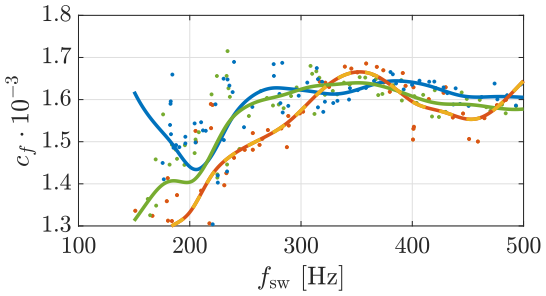

(b) Zoomed in view of the frequency range below 500 Hz

Fig. 3: Performance metric c_f as a function of the switching frequency f_{sw} for horizon combinations $N = \{1, 1\}, \{2, 2\}, \{5, 2\}$ and $\{5, 5\}$. The individual simulations are indicated with dots and their trend is approximated using polynomials.

outperforms a shorter one (e.g., combinations $N = \{1, 1\}$ and $N = \{2, 2\}$) in terms of c_f, with the exception of a small frequency range around 350 Hz. Therefore, it is evident that, as also reported [1], [3], a long horizon improves the drive performance, whether the conventional combination $N = \{5, 5\}$, i.e., $N_p = N_c$, or the proposed configuration—where $N_p > N_c$—is used. Moreover, it is worth mentioning that c_f is lower for $f_{\text{sw}} \leq 500$ Hz, implying a favorable drive performance for this range of switching frequencies. This is due to the higher granularity of switching, since the sampling-to-switching frequency ratio is high, and close to 100, which is the desired ratio [1, Section V]. Finally, an important remark is that FCS-MPC with the horizon combination $N = \{5, 2\}$ achieves the exact same steady-state performance—in terms of c_f—as with $N = \{5, 5\}$, for up to almost 800 Hz. Hence, it can be deduced that long-horizon FCS-MPC with the proposed objective function (6) fully utilizes the advantages associated with long horizons, see [1, Section VI]. Therefore, only $N = \{5, 2\}$ and $N = \{1, 1\}$ are analyzed and compared in the following sections.

IV. Robustness Analysis

Depending on the motor operating point, its parameters can vary considerably, e.g., as a function of the motor temperature for resistances, or under the effect of magnetic saturation for reactances. To identify the most important parameters for an estimation algorithm design, the effect of the parameter

TABLE I: MV system parameters.

Parameter	Value
Rated voltage V_R	3300 V
Rated current I_R	356 A
Real power P_R	1.646 MW
Apparent power S_R	2.035 MVA
Angular stator frequency ω_{sR}	$2\pi 50$ rad/s
Rotational speed ω_{mR}	596 rpm
Number of pole pairs p	5
Stator resistance R_s	$57.61m\,\Omega$
Rotor resistance R_r	$48.89m\,\Omega$
Stator leakage inductance L_{ls}	2.544 mH
Rotor leakage inductance L_{lr}	1.881 mH
Main inductance L_m	40.01 mH
Dc-link voltage V_{dc}	5.2 kV

mismatches in the prediction model on the performance metric c_f of the proposed FCS-MPC is examined. To this aim, $\pm 50\%$ variations in X_{ls}, X_{lr}, X_m, R_s, and R_r are studied for the chosen horizon combinations, and the IM operation at the rated speed and torque is assumed for all simulations.

The results in Figs. 4(a), 4(b) and 4(c) show that, regardless of the horizon combination, variations in X_{ls} and X_{lr} clearly detract from the controller performance metric, whereas mismatches in X_m change it only slightly. Moreover, it is seen that underestimated reactances lead to more substantial performance deviations from the nominal behavior. On the other hand, as shown in Figs. 4(d) and 4(e), variations in the stator and rotor resistances have a negligible effect on the performance metric c_f, mainly due to their typically very small value in MV drives.

The presented results are reasonable since an IM can be considered as a load with essentially inductive behavior, where the reactances can be modeled by the total leakage reactance X_σ (3c). Note that the latter is mainly sensitive to deviations in the stator and rotor leakage reactances, see [20]. Hence, it can be concluded that the mutual reactance as well as the stator and rotor resistances can be excluded from consideration when designing the estimation algorithm. On the other hand, the FCS-MPC robustness can be significantly improved by correctly estimating X_{lr} and X_{ls}, and updating the prediction model accordingly. However, as mentioned in Section II, owing to the adopted inverse-Γ model, only the total leakage reactance X_σ needs to be accurately estimated to address the adverse effects of mismatches in X_{ls} and X_{lr}. The estimation algorithm developed in Section V exploits this fact.

V. Estimator Design

Motivated by the robustness analysis results, a simple estimation method is introduced in the following. By assuming that the stator R_s and rotor R_r resistances are approximately zero—which is a valid assumption for MV machines [16]—the inverse-Γ-equivalent model in Fig. 2(b) can be represented as in Fig. 5(a), where $\boldsymbol{v}_{\text{emf}}$ is the back electromotive force (back-EMF). The differential equation that describes the dynamics of the stator current is

$$\hat{X}_\sigma \frac{\mathrm{d}\boldsymbol{i}_s(t)}{\mathrm{d}t} = \boldsymbol{v}_s(t) - \boldsymbol{v}_{\text{emf}}(t), \tag{8}$$

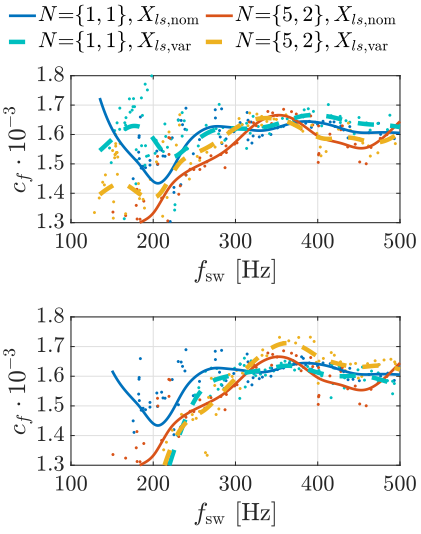

(a) A +50% (up) and −50% (down) variation in the stator leakage reactance X_{ls}

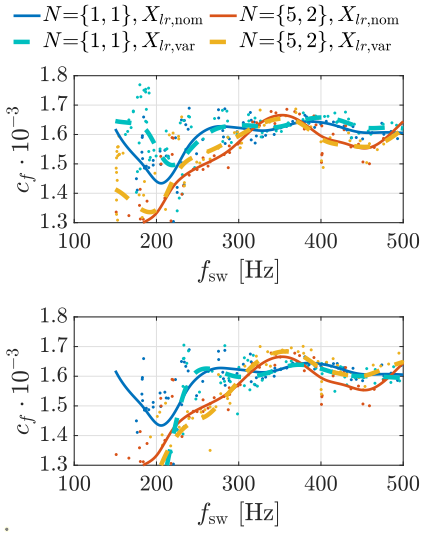

(b) A +50% (up) and −50% (down) variation in the rotor leakage reactance X_{lr}

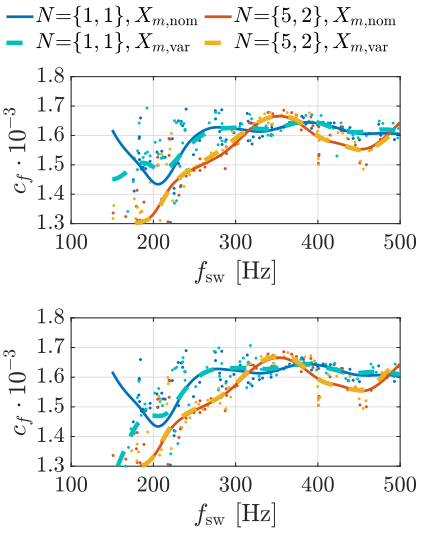

(c) A +50% (up) and −50% (down) variation in the mutual reactance X_m

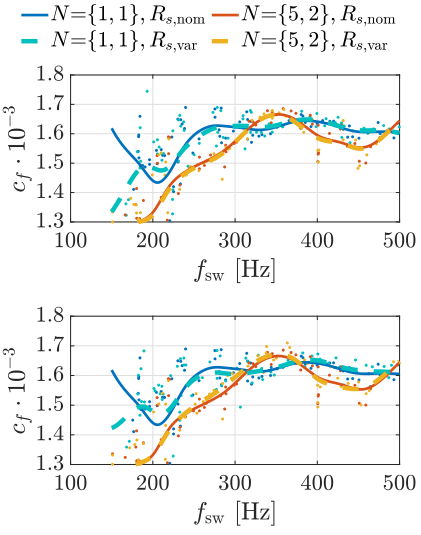

(d) A +50% (up) and −50% (down) variation in the stator resistance R_s

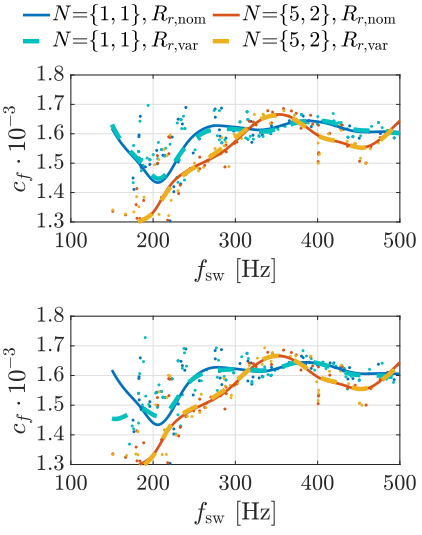

(e) A +50% (up) and −50% (down) variation in the rotor resistance R_r

Fig. 4: Performance metric c_f as a function of the switching frequency f_{sw} for horizon combinations N={1, 1} and {5, 2}. The individual simulations are indicated with dots and their trend is approximated using polynomials.

where $\hat{X}_\sigma$ denotes the total leakage reactance value to be estimated and used in the prediction model (5).

The estimation algorithm is based on the assumption that the back-EMF is sinusoidal and its amplitude remains constant during the sampling interval T_s, see Fig. 5(b). Given this, the total leakage reactance $\hat{X}_\sigma$ can be devised from

$$\|\boldsymbol{v}_{\text{emf}}(k)\|_2^2 - \|\boldsymbol{v}_{\text{emf}}(k-1)\|_2^2 = v_{\text{emf},\alpha}^2(k) + v_{\text{emf},\beta}^2(k) - v_{\text{emf},\alpha}^2(k-1) - v_{\text{emf},\beta}^2(k-1) = 0\,. \tag{9}$$

Each term in (9) can be found by discretizing (8) with the forward Euler method, i.e.,

$$v_{\text{emf},z}(\ell) = (\hat{X}_\sigma \Delta A_z(\ell+1) + v_{sz}(\ell))^2\,, \tag{10}$$

where

$$\Delta A_z(\ell{+}1) = -\frac{i_{sz}(\ell+1) - i_{sz}(\ell)}{T_s}\,, \tag{11}$$

with $z \in \{\alpha, \beta\}$, and $\ell \in \{k, k-1\}$. For example, for $z = \alpha$ and $\ell = k-1$, $v_{\text{emf},\alpha}(k{-}1)$ is calculated as

$$v_{\text{emf},\alpha}(k-1) = \left(-\hat{X}_\sigma \cdot \frac{i_{s\alpha}(k) - i_{s\alpha}(k-1)}{T_s} + v_{s\alpha}(k-1)\right)^2\,. \tag{12}$$

With the help of (10) and (11), (9) can be written in the form of the following quadratic equation [21]

$$\hat{X}_\sigma^2 A + \hat{X}_\sigma B + C = 0\,, \tag{13}$$

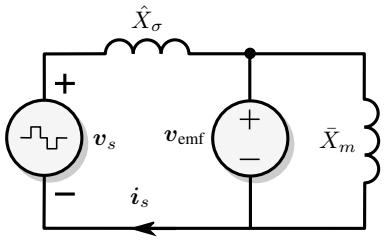

(a) Simplified equivalent model of an IM

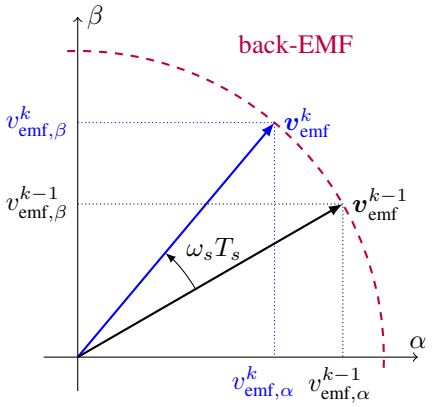

(b) Representation of the back-EMF

Fig. 5: Principle of the proposed estimation algorithm.

where

$$A = \Delta A_\alpha^2(k+1) + \Delta A_\beta^2(k+1) - \Delta A_\alpha^2(k) - \Delta A_\beta^2(k)\,, \tag{14a}$$

$$B = 2\Big(\Delta A_\alpha(k+1)v_{s\alpha}(k) + \Delta A_\beta(k+1)v_{s\beta}(k) - \Delta A_\alpha(k)v_{s\alpha}(k-1) - \Delta A_\beta(k)v_{s\beta}(k-1)\Big)\,, \tag{14b}$$

$$C = v_{s\alpha}^2(k) + v_{s\beta}^2(k) - v_{s\alpha}^2(k-1) - v_{s\beta}^2(k-1)\,. \tag{14c}$$

After substituting (14) into (13), the total leakage reactance is calculated with

$$\hat{X}_{\sigma 1,2} = \frac{B}{2A}\left[-1 \pm \sqrt{1 - \frac{4CA}{B^2}}\right], \tag{15}$$

where the meaningful root is kept. The criterion for the latter is based on the assumption that the back-EMF vector $\boldsymbol{v}_{\text{emf}}$ rotates counterclockwise by the angle corresponding to one sampling interval when the correct value of $\hat{X}_\sigma$ is used, i.e.,

$$\varphi = \omega_s T_s\,, \tag{16}$$

with ω_s being the stator angular speed.

To implement the root-choosing criterion for (15), the two possible angles between the back-EMF vectors at two consecutive sampling intervals—$\boldsymbol{v}_{\text{emf}}(k-1)$ and $\boldsymbol{v}_{\text{emf}}(k)$—are calculated with

$$\varphi_{\sigma 1,2} = \arccos\left(\frac{\boldsymbol{v}_{\text{emf}1,2}(k)^T \boldsymbol{v}_{\text{emf}1,2}(k-1)}{\|\boldsymbol{v}_{\text{emf}1,2}(k)\|_2 \|\boldsymbol{v}_{\text{emf}1,2}(k-1)\|_2}\right). \tag{17}$$

Note that in (17), the values of the back-EMF vectors are computed by substituting the two possible values of $\hat{X}_\sigma$, i.e., $\hat{X}_{\sigma 1,2}$, from (15) into (10). Finally, the angles from (17) are compared with (16), and $\hat{X}_\sigma$ is chosen based on the smallest difference $|\varphi_{\sigma 1,2} - \varphi|$.

Algorithm 1 Update X_σ^{pred}

if $B = 0$ **or** $C = 0$ **or** $4CA/B^2 > 1$ **then**
  $X_\sigma^{\text{pred}} \leftarrow X_\sigma^{\text{pred}}(k-1)$
  return
end if
calculate $\hat{X}_{\sigma 1,2}$ from (15) and $|\varphi_{\sigma 1,2} - \varphi|$ with the help of (17)
if $|\varphi_{\sigma 1} - \varphi| < |\varphi_{\sigma 2} - \varphi|$ **then**
  $\hat{X}_\sigma \leftarrow \hat{X}_{\sigma 1}$
else
  $\hat{X}_\sigma \leftarrow \hat{X}_{\sigma 2}$
end if
$X_\sigma^{\text{pred}} \leftarrow \hat{X}_\sigma$

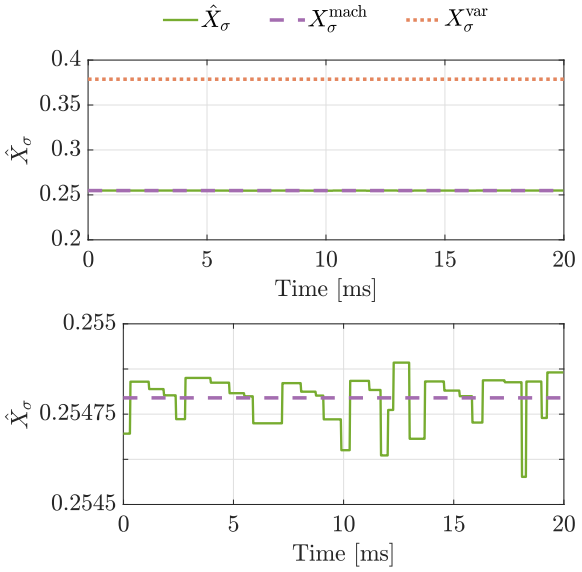

Fig. 6: Estimated values of $\hat{X}_\sigma$ over one fundamental period (up) and its zoomed in view (down). A variation of $+50\%$ is simultaneously introduced in both X_{ls} and X_{lr}, resulting in the wrong value of $X_\sigma^{\text{var}} = 0.38\,\text{p.u.}$, whereas the actual machine reactance is $X_\sigma^{\text{mach}} = 0.2548\,\text{p.u.}$

Further analysis of (15) reveals supplementary conditions which have to be addressed in order to guarantee feasibility of the estimation algorithm results. Specifically, when a switch position does not change between two consecutive sampling intervals, i.e., $\boldsymbol{u}_{abc}(k) = \boldsymbol{u}_{abc}(k-1)$, (14b) is often equal to zero, thus leading to an incorrect calculation. Moreover, if a change in the switch position results in a stator voltage vector of the same amplitude as the one last applied, i.e., $\|\boldsymbol{v}_s(k)\|_2 = \|\boldsymbol{v}_s(k-1)\|_2$, then (14c) gives zero. As a result, for the given system parameters (see Table I), an estimation error of about 15% is observed at some time instants. Additionally, cases where the root in (15) is negative are excluded from consideration in the estimation algorithm.

Altogether, the above-mentioned conditions are summarized

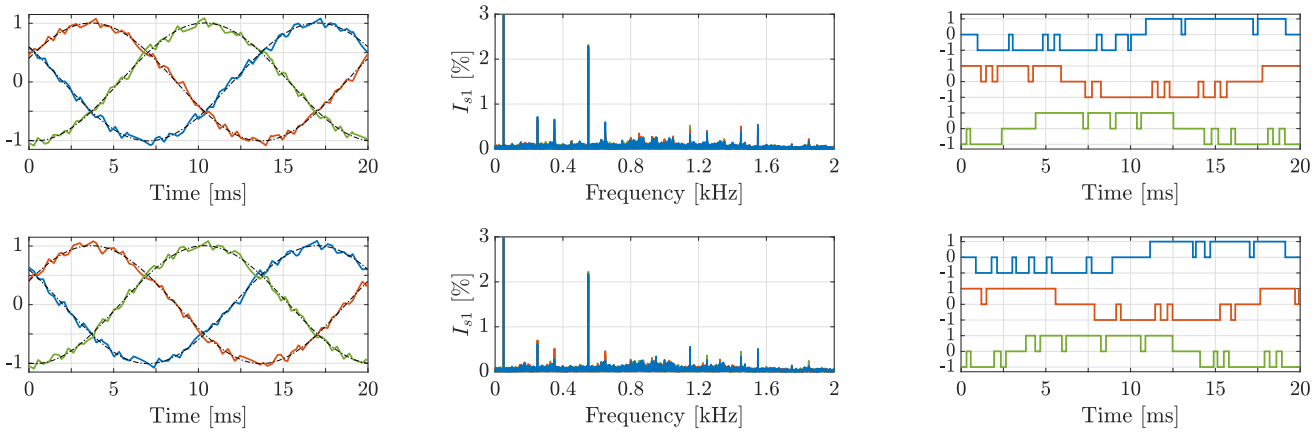

(a) Three-phase stator current $\boldsymbol{i}_{s,abc}$ (solid lines) and their references (dash-dotted lines)

(b) Stator current spectrum. The THD is 5.95%

(c) Three-phase switch position $\boldsymbol{u}_{abc}$

Fig. 7: Simulation results with the proposed FCS-MPC augmented with the estimation algorithm during steady-state operation for a simultaneous variation in both X_{ls} and X_{lr}. Top row: $+50\%$ variation in X_{ls} and X_{lr}. Bottom row: -50% variation in X_{ls} and X_{lr}. The switching frequency is $f_{\text{sw}} = 250$ Hz by setting $\lambda_u = 0.038$, and the prediction and control horizons are $N_p = 5$ and $N_c = 2$, respectively.

in Algorithm 1. In the end, these special conditions force the estimator to be idle, i.e., to use the value of the total leakage reactance from the previous step $X_\sigma^{\text{pred}}(k-1)$, for the biggest part of the fundamental period, namely around 95% of the time for the chosen value of T_s, see the bottom figure in Fig. 6. It is important to point out, however, that this is acceptable, since due to the slower changes in the total leakage reactance compared to the stator current dynamics, the reactance value used in the prediction model X_σ^{pred} does not need to be updated with a new estimation $\hat{X}_\sigma$ at every iteration of the MPC algorithm.

VI. Estimator Performance Evaluation

The effectiveness of the proposed estimation scheme is demonstrated by the time- and frequency-domain results presented in this section, see Fig. 7. By simultaneously varying both leakage reactances, X_{ls} and X_{lr} by $\pm 50\%$, variations of approximately $\pm 50\%$ in the total leakage reactance X_σ are introduced [20]. The tests performed relate to the VSD system shown in Fig. 1, with the parameters in Table I, while $N = \{5, 2\}$ and $T_s = 25\,\mu$s are chosen. All results in this section are shown in the p.u. system.

In the presence of these mismatches, the proposed estimation scheme manages to estimate the correct value of X_σ, update the prediction model accordingly, and, thus, ensure that the FCS-MPC will remain robust to variations in the leakage reactances, as also verified in Figs. 8 and 9. Specifically, Figs. 8(a) and 9(a) show how the mismatches detract from the controller performance with nominal parameters. As can be seen, underestimating the reactances results in more significant deviations in c_f compared with overestimating them, which is in line with the results in Section IV.

On the other hand, the FCS-MPC scheme performance seems immune to any parameter mismatches when the estimation algorithm is activated regardless of the degree of the said mismatches, see Figs. 8(b) and 9(b). These figures, clearly demonstrate the effectiveness of the proposed estimation algorithm, which in conjunction with the designed FCS-MPC algorithm, result in a favorable drive behavior. Finally, it is important to mention that the estimation scheme, and subsequently the FCS-MPC algorithm, do not need to know which leakage reactance is changed and by how much, since, thanks to the adopted modeling, only knowledge of X_σ is required. It can be concluded that this provides the proposed controller with a high degree of robustness.

VII. Conclusions

This paper proposed a long-horizon FCS-MPC algorithm for IM MV drives with (a) reduced computational complexity, and (b) enhanced robustness to parameter variations and mismatches. As shown, the former is achieved by tailoring the optimization problem to the needs of the chosen case study. The latter is fulfilled by appropriately modeling the drive system which allows for an effective estimation algorithm with low computational load. The presented results based on a three-level NPC inverter driving an MV IM demonstrated the effectiveness of the proposed approach, where a superior drive performance is achieved and maintained, even in the presence of significant variations in the system parameters.

Acknowledgments

The authors would like to gratefully acknowledge the financial support from the Myron Zucker Student-Faculty Grant Program established within the IEEE Foundation and administered by the IEEE Industry Applications Society.

References

[1] P. Karamanakos and T. Geyer, "Guidelines for the design of finite control set model predictive controllers," *IEEE Trans. Power Electron.*, vol. 35, no. 7, pp. 7434–7450, Jul. 2020.

[2] P. Cortés, M. P. Kazmierkowski, R. M. Kennel, D. E. Quevedo, and J. Rodríguez, "Predictive control in power electronics and drives," *IEEE Trans. Ind. Electron.*, vol. 55, no. 12, pp. 4312–4324, Dec. 2008.

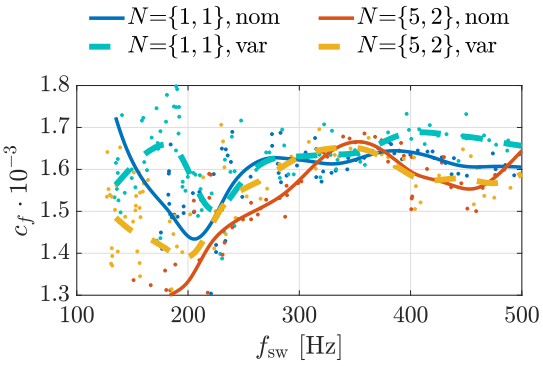

(a) Without the estimation algorithm

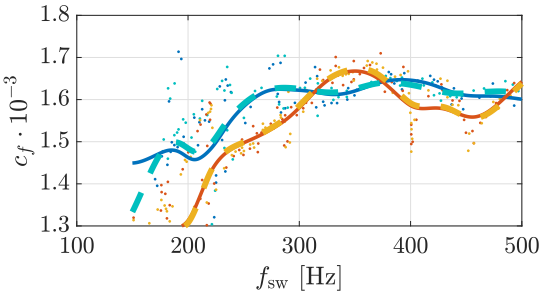

(b) With the estimation algorithm

Fig. 8: Performance metric c_f as a function of the switching frequency f_{sw} for horizon combinations $N = \{1, 1\}$ and $\{5, 2\}$ for the nominal parameters and for a $+50\%$ simultaneous variation in both X_{ls} and X_{lr}. The individual simulations are indicated with dots and their trend is approximated using polynomials.

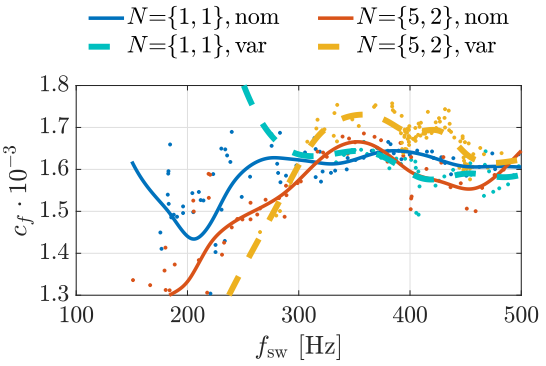

(a) Without the estimation algorithm

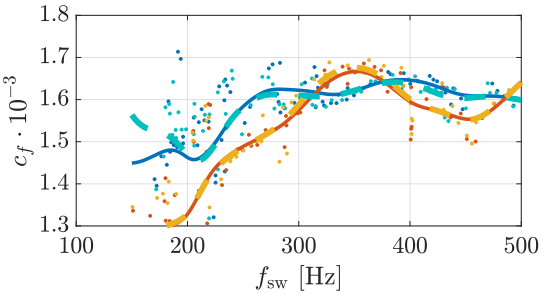

(b) With the estimation algorithm

Fig. 9: Performance metric c_f as a function of the switching frequency f_{sw} for horizon combinations $N = \{1, 1\}$ and $\{5, 2\}$ for the nominal parameters and for a -50% simultaneous variation in both X_{ls} and X_{lr}. The individual simulations are indicated with dots and their trend is approximated using polynomials.

[3] T. Geyer, P. Karamanakos, and R. Kennel, "On the benefit of long-horizon direct model predictive control for drives with LC filters," in *Proc. IEEE Energy Convers. Congr. Expo.*, Pittsburgh, PA, USA, Sep. 2014, pp. 3520–3527.

[4] T. Geyer and D. E. Quevedo, "Multistep finite control set model predictive control for power electronics," *IEEE Trans. Power Electron.*, vol. 29, no. 12, pp. 6836–6846, Dec. 2014.

[5] P. Karamanakos, T. Geyer, N. Oikonomou, F. D. Kieferndorf, and S. Manias, "Direct model predictive control: A review of strategies that achieve long prediction intervals for power electronics," *IEEE Ind. Electron. Mag.*, vol. 8, no. 1, pp. 32–43, Mar. 2014.

[6] P. Karamanakos, E. Liegmann, T. Geyer, and R. Kennel, "Model predictive control of power electronic systems: Methods, results, and challenges," *IEEE Open J. Ind. Appl.*, vol. 1, pp. 95–114, 2020.

[7] G. Betti, M. Farina, and R. Scattolini, "A robust MPC algorithm for offset-free tracking of constant reference signals," *IEEE Trans. Autom. Control*, vol. 58, no. 9, pp. 2394–2400, Sep. 2013.

[8] L. Yan, F. Wang, M. Dou, Z. Zhang, R. Kennel, and J. Rodríguez, "Active disturbance-rejection-based speed control in model predictive control for induction machines," *IEEE Trans. Ind. Electron.*, vol. 67, no. 4, pp. 2574–2584, Apr. 2020.

[9] L. Yan and X. Song, "Design and implementation of Luenberger model-based predictive torque control of induction machine for robustness improvement," *IEEE Trans. Power Electron.*, vol. 35, no. 3, pp. 2257–2262, Mar. 2020.

[10] O. Wallscheid and E. F. B. Ngoumtsa, "Investigation of disturbance observers for model predictive current control in electric drives," *IEEE Trans. Power Electron.*, vol. 35, no. 12, pp. 13 563–13 572, Dec. 2020.

[11] J. L. Zamora and A. Garcia-Cerrada, "Online estimation of the stator parameters in an induction motor using only voltage and current measurements," *IEEE Trans. Ind. Appl.*, vol. 36, no. 3, pp. 805–816, May/Jun. 2000.

[12] M. Yang, X. Lang, J. Long, and D. Xu, "Flux immunity robust predictive current control with incremental model and extended state observer for PMSM drive," *IEEE Trans. Power Electron.*, vol. 32, no. 12, pp. 9267–9279, Dec. 2017.

[13] X. Zhang, L. Zhang, and Y. Zhang, "Model predictive current control for PMSM drives with parameter robustness improvement," *IEEE Trans. Power Electron.*, vol. 34, no. 2, pp. 1645–1657, Feb. 2019.

[14] C.-K. Lin, J.-t. Yu, Y.-S. Lai, and H.-C. Yu, "Improved model-free predictive current control for synchronous reluctance motor drives," *IEEE Trans. Ind. Electron.*, vol. 63, no. 6, pp. 3942–3953, Jun. 2016.

[15] F. Tinazzi, P. G. Carlet, S. Bolognani, and M. Zigliotto, "Motor parameter-free predictive current control of synchronous motors by recursive least square self-commissioning model," *IEEE Trans. Ind. Electron.*, vol. 67, no. 11, pp. 9093–9100, Nov. 2020.

[16] T. Geyer, *Model predictive control of high power converters and industrial drives*. Hoboken, NJ, USA: Wiley, 2016.

[17] A. M. Alturas, S. M. Gadoue, B. Zahawi, and M. A. Elgendy, "On the identifiability of steady-state induction machine models using external measurements," *IEEE Trans. Energy Convers.*, vol. 31, no. 1, pp. 251–259, Mar. 2016.

[18] G. Slemon, "Modelling of induction machines for electric drives," *IEEE Trans. Ind. Appl.*, vol. 25, no. 6, pp. 1126–1131, Nov./Dec. 1989.

[19] P. Karamanakos, T. Geyer, and R. Kennel, "A computationally efficient model predictive control strategy for linear systems with integer inputs," *IEEE Trans. Control Syst. Technol.*, vol. 24, no. 4, pp. 1463–1471, Jul. 2016.

[20] L. Ortombina, P. Karamanakos, and M. Zigliotto, "Robustness Analysis of Long-Horizon Direct Model Predictive Control: Induction Motor Drives," in *2020 IEEE 21st Work. Control Model. Power Electron.* IEEE, Nov. 2020, pp. 1–8.

[21] B. Arif, L. Tarisciotti, P. Zanchetta, J. C. Clare, and M. Degano, "Grid parameter estimation using model predictive direct power control," *IEEE Trans. Ind. Appl.*, vol. 51, no. 6, pp. 4614–4622, Nov./Dec. 2015.